Materials and Design 74 (2015) 67–75

Contents lists available at ScienceDirect

Materials and Design

journal homepage: www.elsevier.com/locate/matdes

Mitigation of abrasive wear damage of Ti–6Al–4V by laser surface alloying

D.I. Adebiyi, A.P.I. Popoola *

Department of Chemical, Metallurgical and Materials Engineering, Tshwane University of Technology, P.M.B. X680, Pretoria 0001, South Africa

ARTICLE INFO

Article history:
Received 28 July 2014
Accepted 14 February 2015
Available online 23 February 2015

Keywords:
Laser alloying
Titanium aluminides
Ti–6Al–4V alloys
Three body abrasive wear resistance

ABSTRACT

Ti–6Al–4V alloy is lightweight, heat treatable and machinable with excellent strength characteristics. These properties favor its extensive applications in the automobile, aerospace and aeronautical industry. However, low hardenability, poor wear resistance and the tendency to gall and smear have reduced the use of Ti–6Al–4V. This study was designed to investigate the enhancement in the abrasive wear resistance of Ti–6Al–4V laser alloyed with three different premixed composition of Mo + Zr + Stellite 6 using a 4.4 kW continuous wave (CW) Rofin Sinar Nd:YAG laser processing system. Microstructural evolution in the samples was studied by optical and scanning electron microscopes. The phase evolution was studied by X-ray diffractometer. There exists metallurgical reaction and bonding between the Ti–6Al–4V substrate and the laser coatings. Scanning electron micrographs and X-ray diffraction spectra of the coatings revealed the formation of various titanium aluminides among other complex phases. The β-phase of Ti was retained owning to the presence of Mo – a β-phase stabilizer, in the powder mixture. Three-body abrasive wear resistance test indicates that the wear of the coatings was dominated by adhesive mechanism which is characterized by fine scratches. A twenty-four fold improvement in wear resistance was obtained in the coatings when compared with the native alloy.

1. Introduction

Since discovered in the early 1950s, titanium and its alloys (Ti–6Al–4V in particular), have become backbone materials for many industries such as the aeronautical, chemical, marine, power generation, sports and leisure, transportation, and biomedical industries, for manufacturing critical systems, and airframes. This is due to the unique combination of many desirable and versatile specific bulk properties of the alloy which include low density that gives rise to very attractive strength-to-weight ratio, high specific strength, low elastic modulus, superior corrosion and erosion resistance in many environments, excellent high temperature resistance and biocompatibility [1–7]. However, despite these numerous laudable properties, poor wear resistance, low hardness, high friction coefficient, low hardenability and the tendency to gall and smear have limited the engineering applications of titanium and its alloys [8–10]. The high coefficient of friction and poor tribological behavior of titanium can be traced to three fundamental factors which are: titanium's atomic structure, crystal structure and the relatively low tensile and shear strength of the titanium oxide film.

Therefore, the need to develop methods that will remove these limitations, improve and enhance the properties of titanium and its alloys while retaining the desirable bulk properties is important for industrial application. In view of the fact that the aforementioned failures of titanium and its alloys are surface dependent rather than the bulk alloy, surface modification holds a promise of improving the surface properties [11]. Surface modification processes that can be successfully applied to efficiently improve the surface dependent properties of titanium and its alloys include laser surface treatment (laser surface alloying, (LSA), laser cladding (LC)), ion implantation, physical vapor deposition (PVD), chemical vapor deposition (CVD), carburizing, nitriding, ion implantation, thermal oxidation heat treatment, shielded metal arc welding and gas tungsten arc welding [12,13].

Laser surface alloying (LSA), can rapidly provide a thick and crack-free layer in all instances with metallurgical bonds at the interface between the alloyed layer and the substrate [1]. In LSA, external alloying elements in form of powder (metal, alloy, ceramic, cermet or intermetallic) are introduced into the surface of a substrate, as pre-placed material or injected directly into the melt pool created on the substrate by a high power laser beam. The melting of the substrate occurs rapidly only at the surface, while the bulk of

* Corresponding author. Tel.: +27 12 382 3513.
E-mail addresses: Adebiyidi@gmail.com (D.I. Adebiyi), PopoolaAPI@tut.ac.za (A.P.I. Popoola).

http://dx.doi.org/10.1016/j.matdes.2015.02.010
0261-3069/

the material remains cool, thus serving as an infinite heat sink. The result of this is rapid self quenching and resolidification of new alloy due to the large temperature gradients between the melted surface region and the underlying solid substrate. One consequence of this is the evolution of a wide variety of microstructures as a result of the rapid cooling from the liquid phase [14,15]. Hence, during laser alloying, the synthesis of new alloy is possible by depositing a premixed ratio of elemental powders. Powders surfaced on new or worn working surfaces of components by LSA provides specific properties such as high abrasive wear resistance, erosion resistance, corrosion resistance, heat resistance and combinations of these properties. Consequently, improvements in machinery performance and safety in aerospace, automotive, can be realized by the method [16]. According to Poulon-Quintina et al. [17], laser beams, because of specific thermal characteristics induced by laser irradiation, can generate specific microstructures including metastable phases and nano-crystalline grains.

Laser processing offers unique and significant quality and cost advantages over traditional techniques. These include high throughput speed, process compatibility, high process efficiency, low porosity and good surface uniformity. In addition, the rapid self quenching in laser alloying results in a true metallurgical bond between the composite layer and substrate, the formation of a non-equilibrium or amorphous phase as well as homogenization and refinement of the microstructure, all without affecting the bulk properties of the substrate [18,19].

A number of investigations have been carried out on the alloying of Ti substrate with a mixture of powders. Fallah et al. [20] used a fiber laser to modify the surface composition of a Ti–6Al–4V plate through deposition of the blown powder mixture of Ti–45 wt%Nb. The authors reported that continuous beads were formed with pore-free sections and a homogeneous composition corresponding to that of β (Ti, Nb) solid solution phase. Three kinds of laser boronizing composite coatings were in situ synthesized on Ti substrate by using powders of B, BN and B_4C as starting materials [19]. Results show the coating has higher microhardness and better wear resistance than pure Ti substrate and the composition, microstructure, microhardness, and wear resistance of the resulting laser boronized composite coatings vary with the composition of the starting materials [21].

Popoola et al. [22] investigated laser coating of commercial titanium alloy with combination of Zr and TiC and reported an increase in the hardness of the substrate. Fogagnolo et al. [1] introduced niobium into the surface layer of titanium by laser surface alloying and reported that the resulting microstructure led to reduction of approximately 30% in Young's modulus and a more than 100% increase in hardness. Ochonogor et al. [23] developed titanium metal matrix composite on titanium alloy and reported that the wear resistance of the alloy improved significantly, indicating a fifteen fold wear rate reduction due to the proper distribution of the ceramic particles. Lin et al. [12] investigated in situ formed TiNx reinforcing phase within the clad layer of Ti–6Al–4V by gas tungsten arc welding (GTAW) and reported that the hardness of the TiN clad layer is two times better, whilst the wear resistance is ten times more than that of the Ti–6Al–4V substrate. Chikarakara et al. [24] reported that high speed laser surface modification of Ti–6Al–4V led to a microhardness increased up to 760 $HV_{0.05}$ which represented a 67% increase compared to the bulk material. Chun et al. [25] fabricated intermetallic compound composite coating on pure Ti substrate by laser and reported that the intermetallic compound coating contributes to greatly increase the microhardness of the pure Ti substrate yielding a high-average hardness which is about four times higher than that of pure Ti substrate. Therefore, the values of wear rate for intermetallic coated samples are nearly two orders of magnitude lower than that of pure Ti substrate.

Molybdenum (Mo) and its alloys have outstanding combination of high temperature properties (such as high melting point, low vapor pressure and high temperature strength), while zirconium (Zr) has a tendency to promote chemical homogenization. Laser alloying with zirconium is suitable to control fretting wear damage [26]. Molybdenum coatings can increase the fretting fatigue strength and prevent material loss during fretting at room and high temperatures. Molybdenum coatings exhibit good corrosion resistance, which is beneficial for fretting resistance [27,28]. Molybdenum is a beta phase stabilizer in titanium while zirconium behaves more as neutral solute and has little effect on the transformation temperature, acting instead as strengthener of the alpha phase [26]. Stellite 6 powder has a unique inherent characteristics of the hard carbide phase dispersed in a CoCr alloy matrix giving it exceptional resistance to wear and many forms of mechanical and chemical degradation over a wide temperature range. In addition, stellite 6 retains a reasonable level of hardness up to 500 °C and resists oxidation up to 1095 °C. It is usually used for alloying due to its high hardness and good bonding strength with the substrate [29,30]. Consequently, a composite coating of premixed ratio of powders of Zr, Mo and stellite 6 formed on titanium is expected to evolve complex microstructure of a stabilized beta phase in the matrix of the titanium, which will enhance the surface properties of the alloy.

Literature exploiting laser to alloy Ti with different premixed powder ratio in order to tailor the predominant phase in the matrix of Ti and evolve complex microstructures that will improve Ti properties is rare. Moreover, there are limited publications that discuss laser alloying of Ti–6Al–4V with pre-mixed ratio of Mo, Zr and stellite 6 powders in order to take advantage of the unique properties of these powders that were discussed above. Hence the process had not been fully understood. Therefore, this research work investigates the abrasive wear damage of titanium alloy by using laser to incorporate different premixed composition of Zr + Mo + stellite 6 on Ti–6Al–4V. Detail and systematic study of the phase evolution and transformation, resultant microstructure, microhardness and abrasive wear resistance behavior of the composite coatings were carried out.

2. Experiments

2.1. Materials and methods

Test pieces cut from as-received (AR) Ti–6Al–4V alloy were used in this investigation. The nominal chemical composition of the alloy is 6.01 wt% Al, 3.84 wt% V, 0.30 wt% Fe, 0.15 wt% Si, 0.10 wt% C, 0.15 wt% O, 0.15 wt% N, Ti, balance. Samples were machined to specimen plates of dimensions ($100 \times 100 \times 6$) mm^3. The plates were sandblasted to clean the surface, minimize reflection of radiation during laser processing and accelerate the absorption of laser energy by the metal. The alloying powder was made up of different compositions of Molybdenum (Mo), Zirconium (Zr) and stellite 6 (S_6) powders. The chemical composition of the stellite 6 powder is 2.26 wt% Fe, 0.28 wt% Mn, 26.48 wt% Cr, 3.26 wt% Ni, 0.068 wt% Nb, 8.095 wt% W, balance Co. The grain size of all the powders used is <45 μm. The powders were weighed separately and then mixed in a vial into three different compositions as shown in Table 1.

Table 1
Composition of the alloying powder.

Sample no	Powder composition
T-M-Zr-S_6 1	50 wt% Mo + 30 wt% Zr + 20 wt% S_6
T-M-Zr-S_6 2	30 wt% Mo + 20 wt% Zr + 50 wt% S_6
T-M-Zr-S_6 3	20 wt% Mo + 50 wt% Zr + 30 wt% S_6

A 4.4 kW Rofin Sinar continuous wave (CW) Nd:YAG laser fitted with an off-axis nozzle for powder feeding was used to generate the laser beam and the alloying process was carried out in two stages which were: the parameter optimization stage and the multiple track alloying stage. The optimization stage was necessary to determine the most suitable set of parameter for the multiple tracks alloying stage. At the optimization stage, preliminary trials of single track alloying were made with different values of laser power, P, scanning speed, s, powder mass flow rate, l, and laser spot diameter, d. These parameters were carefully selected to ensure the supply of sufficient laser energy to the work piece for the dissolution of the powders. The alloyed coating of the first stage was characterized to determine the most suitable set of processing parameters to be used for the multiple track process. Decision was based on the set of parameters which combines high hardness value with homogenous, pores and cracks free composite microstructure in which the reinforcement powder particles were uniformly distributed in the matrix of the substrate. During the multiple tracks laser alloying stage, parallel laser tracks, in which 50% of the previous track was overlapped by the subsequent track, were made. This is necessary to compromise between surface treatment efficiency and homogeneity in properties of the alloyed layer. The laser processing parameters used for the multiple tracks alloying, as obtained after the optimization stage, were as follows: laser power, $P = 4$ kW, scan speed, $V = 0.014$ m/s, laser beam diameter (spot size), $d = 4$ mm. In both stages, laser processing was conducted in an atmosphere of argon gas flowing at 3 L/min to prevent oxidation of the metal through reaction with oxygen, and also to avoid formation of pores due to excessive dissolution of nitrogen. This is essential because Ti–6Al–4V has a high affinity for oxygen and absorption of oxygen will result in the formation of an extremely hard, brittle oxygen-stabilized alpha phase layer known as alpha case.

2.2. Sample preparation and characterization

After laser treatment, the alloyed plates were cross sectioned by mechanical cutting under flowing cooling solution and prepared for characterization. The AR and unabraided coated samples were prepared for metallographic analysis following standard polishing procedure [31] using Kroll's reagent (6 ml HNO_3 + 2 ml HF + 92 ml H_20) as the etchant. The samples were polished sequentially using 80, 120, 320, 400, 500, 600, 800, 1000 μm grades of SiC abrasive paper. This was followed by cloth polishing with 6 μm, 3 μm, 1 μm, 0.5 μm diamond suspensions. There was no surface preparation of the abraded samples prior to characterization. Microstructural evolution was studied by optical microscopy, X-ray diffraction (XRD) and scanning electron microscopy (SEM) equipped with energy dispersed spectrometry (EDS). Phase composition studies was carried out using Philips PW 1713 X-ray diffractometer (XRD) fitted with monochromatic Cu Kα radiation set at 40 kV and 20 mA, while phase identification was done using Philips Analytical X'Pert High Score® software fitted with an inbuilt International Centre for Diffraction Data (ICSD) database. The scan was taken for the 2θ range of 10–80° with a step of 0.02°.

2.3. Microhardness and abrasion tests

A Matsuzawa Seiki Vickers hardness tester was used to measure the microhardness of the alloyed specimens by making a through-thickness hardness profile indentations from the surface of the alloyed zone through to the substrate. A load of 100 g dwelling for 15 s at 100 μm interval between corresponding indentations was used. Ten indentations were made and the average is reported as the hardness of the sample. Three-body abrasion test was carried out in accordance with the standard practice and requirements of the ASTM: G65-04 as shown in Fig. 1.

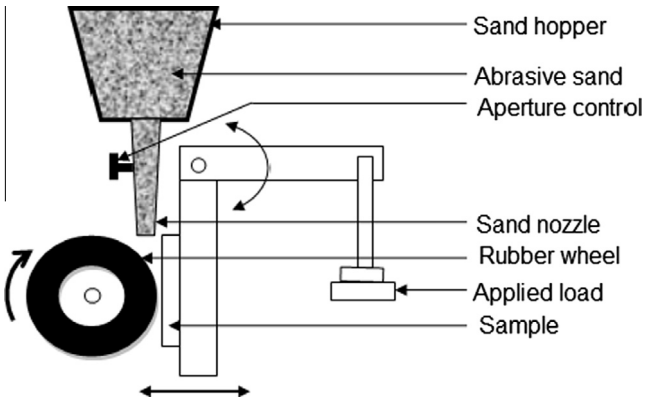

Fig. 1. Schematic diagram of the abrasion wear resistance test machine according to the ASTM: G65-04 standard.

Silica sand obtained from Rolfes (Pty) Limited was used as the abrasive. The silica sand has a particle size range of 0.3–0.65 mm. The particle size and distribution of the silica sand was determined before the wear testing by sieving it with a MACSALAB electronic sieve shaker. The sand particles were generally angular in shape of which a larger proportion reported to the 500–600 μm range and having a D_{50} of 525 μm. In order to remove any unmelted powder and to ensure a common roughness as starting reference, the surface of samples were prepared by grinding with 1200 μm grit SiC abrasive papers. Necessary caution was however taken to prevent removal of the alloyed layer. The sand was delivered at a feed rate of 4.3 g/s by a nozzle positioned between the examined test piece and the rubber wheel in the test chamber. The sand flows in the same direction as that of the rotation of the contact face of the wheel. The flow rate of the sand and rotational speed of the wheel were kept constant for each experiment. The flow rate of the sand is chosen to ensure that sufficient sand is used. The samples were abraded for 30 min, but the test was stopped at 5 min interval to record the weight loss. This is also necessary to prevent excessive heating of the sample and the rubber wheel. A force of 25 N was applied to press the specimen to the rubber wheel. The force was kept constant while the rubber wheel was rotating at a constant speed of 250 rpm. The rotational speed of the wheel and total number of revolution were chosen to ensure appreciable wear of the samples. The specimens were thoroughly cleaned with acetone in an ultrasonic cleaner and weighed before and after the wear test using an electronic balance with a resolution of ±0.01 mg as required by ASTM: G65-04. Two specimens were used for each sample and the average of each sample was taken. The wear was measured by the loss in weight, which was then converted into wear volume. The specific wear rate was determined from weight loss data. JEOL JSM-840 scanning electron microscope in secondary and backscattered electrons imaging modes and EDS chemical element mapping was used to examine the worn surfaces after the abrasion in order to investigate the mechanism of material removal. The porosity of the specimen was determined by Archimedes' principle.

3. Results and discussion

3.1. Results

The hardness result, the phases obtained in the alloyed zone, and the crystallographic structure of the titanium in the composite matrix is presented in Table 2. The result shows that all the powder

Table 2
Coatings properties.

Sample	Powder composition	Microhardness ($HV_{0.1}$)	Compound name	Chemical formula and titanium structure
As-received	–	373.3	–	(α + β)-Ti
1	50 wt% Mo + 30 wt% Zr + 20 wt% S_6	1145.2	Titanium Titanium aluminide Titanium vanadium Niobium tungsten	α-Ti (α-phase) TiAl (α-phase) Ti_{84} V_{16} (ω-phase) NbW β-$TiCo_2Al$ (β-phase) ZrMo (β-phase)
2	30 wt% Mo + 20 wt% Zr + 50 wt% S_6	1022.5	Titanium Titanium aluminide Titanium cobalt Titanium aluminide	α-Ti (α-phase) Ti_5Al TiCo (β-phase) $TiAl_3$ (α-phase) AlTiV (Tetragonal)
3	20 wt% Mo + 50 wt% Zr + 30 wt% S_6	994.7	Titanium Titanium aluminide Nickel vanadium Titanium vanadium Titanium cobalt	α-Ti (α-phase) Ti_5Al (α-phase) NiV_5 Ti_{84} V_{16} (ω-phase) TiCo (β-phase)

compositions used led to improvement in the surface hardness and abrasive wear resistance of the coating. Alloying with a 50 wt% Mo + 30 wt% Zr + 20 wt% S_6 yielded the highest hardness. As shown in the table, different intermetallic phases dominated by titanium aluminides were formed in the composites coating. Among the phases observed were TiCo, NbW, $TiCo_2Al$, TiAl, $TiAl_2$, $TiAl_3$, Ti_5Al.

Fig. 2 is the optical micrograph of the AR titanium (Ti–6Al–4V) and the coated samples. The AR is the two-phase, alpha–beta (α + β) titanium alloy having a Widmanstätten structure (Fig. 2(a)). At room temperature, the alloy is usually characterized by a granular microstructure of α-phase lamellae in the β-matrix. The alpha (α) grains which are light and near equiaxed in shaped are well distributed in the lamellar matrix of the dark beta phase. In the Ti–6Al–4V alloy, aluminum and oxygen are present in trace amount and their presence contribute to stabilizing and strengthening the alpha (α)-phase. This is advantageous for improving hardenability and increasing strength [32]. The laser coatings have porosity of 3 ± 1%, and are relatively defect free as shown by the optical micrograph in Fig. 2(b)–(d). The scanning electron micrographs (SEM) of the AR and samples laser alloyed with the various powder compositions are shown in Fig. 3 while the X-ray diffraction (XRD) spectrums are shown in Fig. 4. Fig. 5 presents the

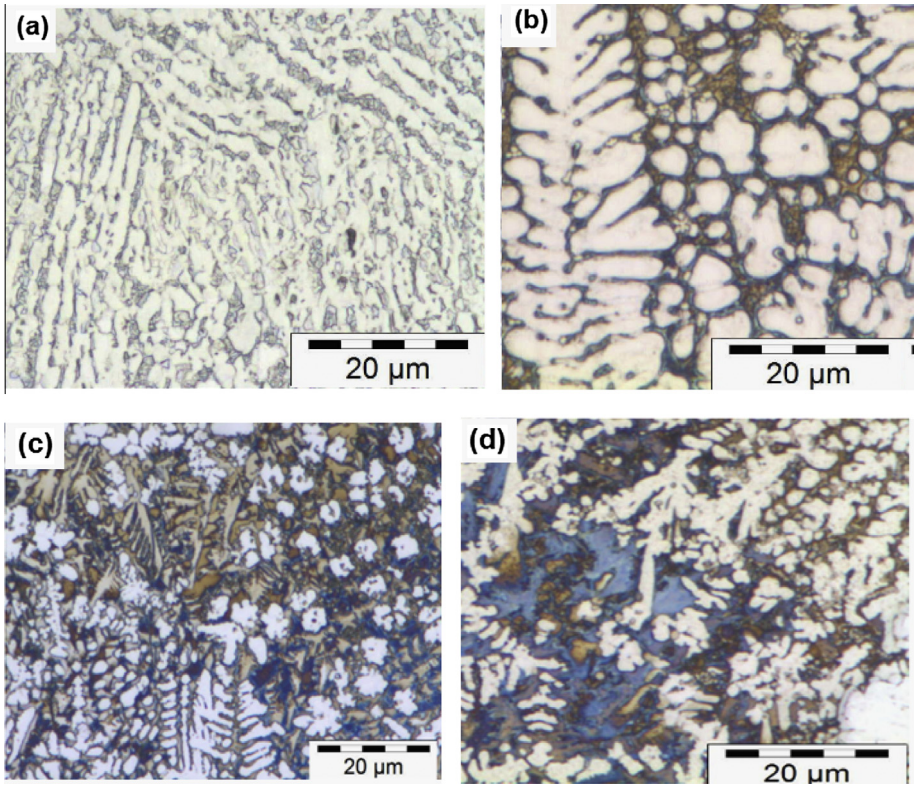

Fig. 2. Optical micrograph of the: (a) alpha–beta titanium alloy (Ti–6Al–4V) showing the typical Widmanstätten structure of white α plates and dark β phase. (b) Cross section of sample 1: 50 wt% Mo + 30 wt% Zr + 20 wt% S_6. (c) Cross section of sample 2: 30 wt% Mo + 20 wt% Zr + 50 wt% S_6. (d) Cross section Sample 3: 20 wt% Mo + 50 wt% Zr + 30 wt% S_6.

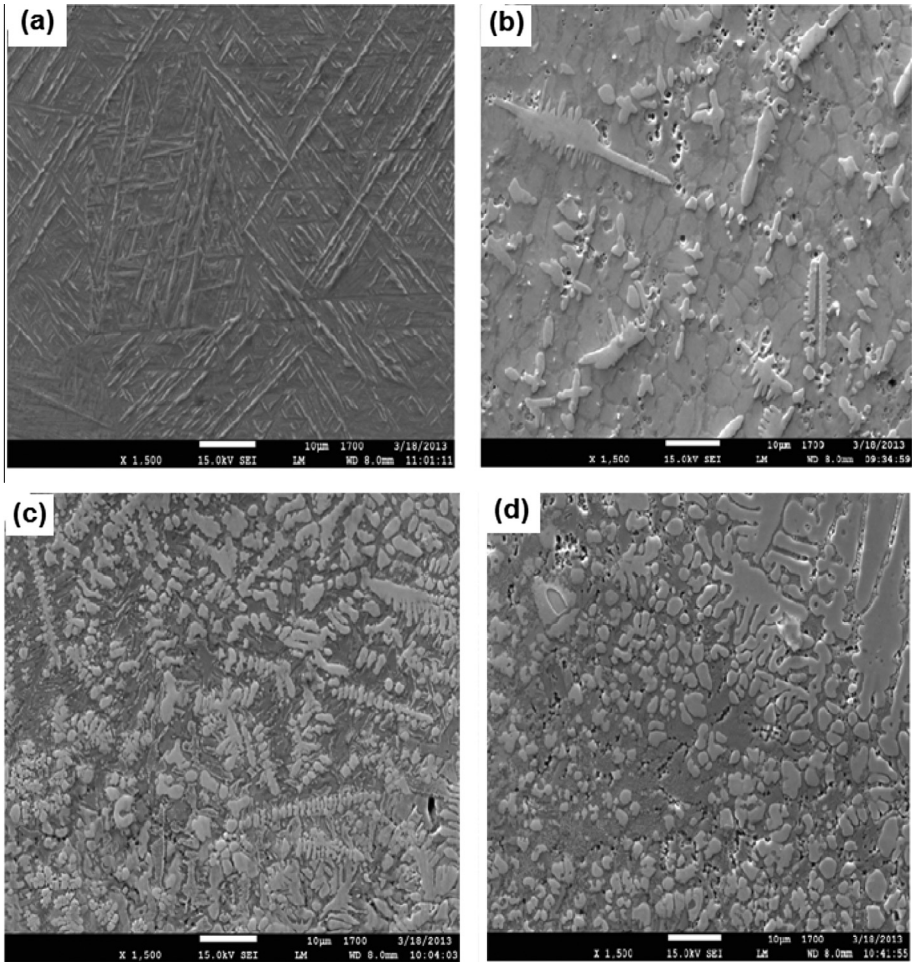

Fig. 3. SEM of: (a) substrate (as-received Ti–6Al–4V alloy) showing its lamellar microstructure. (b) Sample 1: 50 wt% Mo + 30 wt% Zr + 20 wt% S_6. (c) Sample 2: 30 wt% Mo + 20 wt% Zr + 50 wt% S_6. (d) Sample 3: 20 wt% Mo + 50 wt% Zr + 30 wt% S_6.

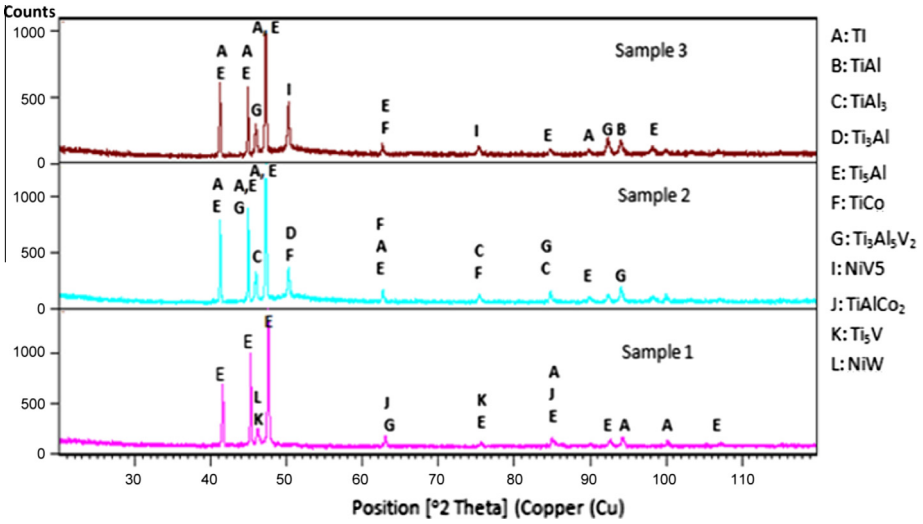

Fig. 4. XRD spectra of the coated samples. Sample 1: 50 wt% Mo + 30 wt% Zr + 20 wt% S_6. Sample 2: 30 wt% Mo + 20 wt% Zr + 50 wt% S_6. Sample 3: 20 wt% Mo + 50 wt% Zr + 30 wt% S_6.

comparison of the Vickers' hardness of the samples whereas Fig. 6 is the histogram showing the overall wear rate of the alloyed surface compared with the native alloy after 30 min of abrasion. The micrographs of the worn surfaces after the abrasion test showing the wear scars and morphology are presented in Fig. 7.

3.2. Discussion

The optical and scanning electron micrographs of coated samples in Figs. 2(b)–(d) and 3(b)–(d) reveal light dendritic structures surrounded by dark interdendritic phases in the matrix of the

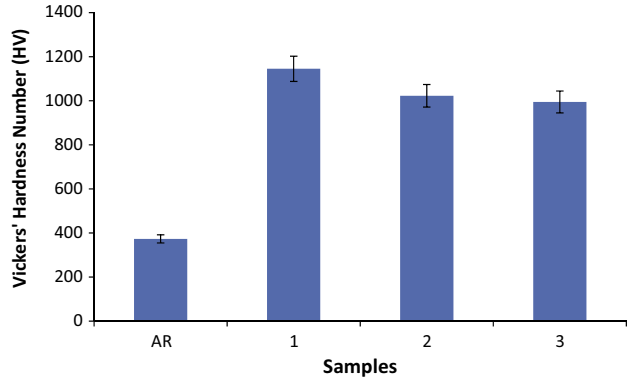

Fig. 5. Vickers hardness of the coated samples.

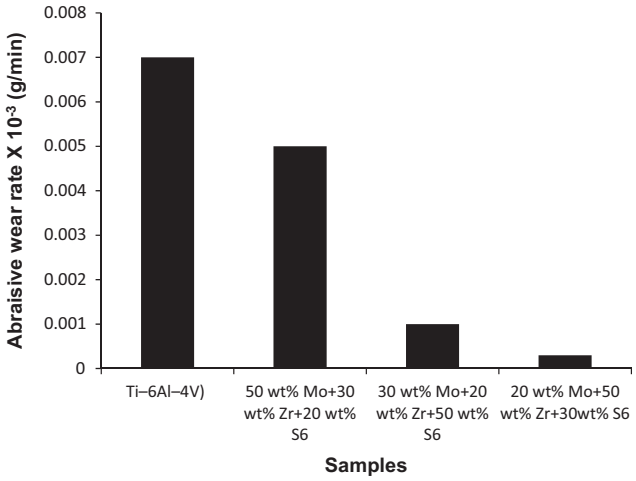

Fig. 6. The wear rates of the titanium matrix composite after 30 min of abrasion.

titanium. This is typical of titanium aluminides [33]. As seen in the SEM (Fig. 2), sample 2 appears to have a higher fraction of the dendrites than other samples. This can be traced to the higher proportion of stellite 6 in the sample. The microstructure of rapidly cooled stellite 6 is known for formation of dendrites [34]. The metal matrix composites (MMCs) formed consist of the newly precipitated Intermetallic phases (IP) and particles of the reinforcement powders. Prominent among the intermetallic phases are TiAl (α-phase), $TiAl_3$ (α-phase), $TiAl_2$, Ti_3Al (α-phase), Ti_5Al (α-phase), Ti_4V (ω-phase), NbW, β-$TiCo_2Al$ (β-phase), ZrMo (β-phase), TiCo (β-phase), AlTiV (tetragonal), NiV_{15}, (ω-phase). The precipitation of these intermetallic phases and complex compounds provides a proof of the dissociation of the powders and the subsequent reaction of the constituents with each other and with the substrate. The formation of the titanium aluminides depends on the value of change in the Gibbs free energy of formation, ΔG_f. Taking the melting point of the titanium alloy as 1660 °C [35], the ΔG_f of the various titanium aluminides is calculated based on the data provided by Chien [36]. The result is presented in Table 3.

The XRD pattern of the coating (Fig. 4) confirms the presence of these intermetallics in the coating. The values of ΔG_f show that $TiAl_3$, $TiAl_2$, Ti_3Al and TiAl would form more readily than Ti_2Al_5, and that the formation of Ti_2Al_5 is non-spontaneous. This is in agreement with the intensities of the XRD spectra. Also, observed in the XRD pattern of all the coated samples are peaks of α-Ti. This could be attributed to the following:

- The abundance of the α-Ti phase in the native alloy.
- The formation of the α-Ti is favored by fast cooling rate which characterizes laser alloying process. This is because, due to fast cooling below β-transus temperature (882 °C), β-phase martensitically transforms to hexagonal close-packed α-phase structure called martensitic α′ which gives higher strength.

The precipitation of the β-phase (β-$TiCo_2Al$), ZrMo (β-phase), TiCo (β-phase) is enhanced by some of the constituents of the powder. Tungsten and cobalt (from the stellite 6), and molybdenum, are β-stabilizing elements. Tungsten and cobalt form a β-isomorphous binary system with titanium while molybdenum forms a β-eutectoid binary system [37]. The evolution of the ω-phase (AlTiV (tetragonal), NiV_{15}, (ω-phase)) is governed by the presence and concentration of the β-stabilizer and the rapid cooling which is a major characteristic of the laser alloying process. In alloys having a specific concentration range of β-stabilizers, rapid cooling from the β-range may yield an athermal ω-phase. The transformation of β to ω due to rapid cooling is martensitic. There is a simultaneous displacement of atoms to a distance not exceeding the interatomic spacing without a change in the composition. In transition-metals alloyed titanium, ω-phase forms when the content of the alloying element satisfies the electron concentration relationship, $e/a = 4.12–4.21$ electrons per atom prior to the start of martensitic transformation. In titanium alloys with β-isomorphic elements, ω-phase appears in the form of fine particles distributed uniformly over the whole of the grain volume [38].

From the hardness results, laser alloying greatly enhanced the surface hardness of the Ti alloy for all the compositions used. The rate of heating and cooling in laser alloying process is usually high, which leads to the refinement in the grain size of the alloyed zones. Thus plays an important role in the enhancement of the properties of the alloyed zones [39]. The powder with the highest Mo contents gave the highest hardness. The general increase in hardness of the alloys can be traced to the presence of molybdenum, zirconium and tungsten (from stellite 6) in the powder mixture, and the evolution of various hard intermetallics of which titanium aluminides are dominant. The hardness of the titanium aluminides intermetallics phases ranges between 2.4 and 2.9 GPa [40]. These intermetallic phases were present in all the coated samples.

The SEM of the worn surface of the AR sample (Fig. 7(a)) shows deep grooves, pronounced damage region and fatigue due to the repeated action of the abrasive particle sand. Also, the evidence of fracture caused by selective removal of alloy, presence of deep scratches, craters, massive damaged spots, pull-outs, delamination of materials from the surface, deep pits and worn out debris were apparent. These can be due to plastic shearing and effect of work hardening. Hence the abrasive mass loss for the AR was very high. A few shallow and surface micro-cracks observed in the micrograph of the uncoated sample show that the deformed material was also progressively detached from the surface of the alloy during abrasion. The scars patterns on the Ti–6Al–4V have patches of colours which suggest that there are hard and soft regions in the material which can be supposed to be due to microstructural heterogeneities. Ti–6Al–4V is a binary alloy consisting of a mixture of stable α phase and metastable β phase. The wear pattern of the titanium alloy is similar to what will be observed on the worn surface of ductile material. Thus explains why the fragmented abrasive SiO_2 particles were observed to be embedded in the worn surfaces (Fig. 7(a)).

In the three-body abrasive wear test, the applied load pushes the sample toward the rubber wheel and the rubber wheel pushes the sand against the sample (Fig. 1). This leads to point indentation of the SiO_2 particles on the specimen. The abrasive wear of the native alloy is dominated by fracture, presence of scratches, delamination of materials from the surface, deep pits, and worn out debris. The as-received can be described to have suffered dam-

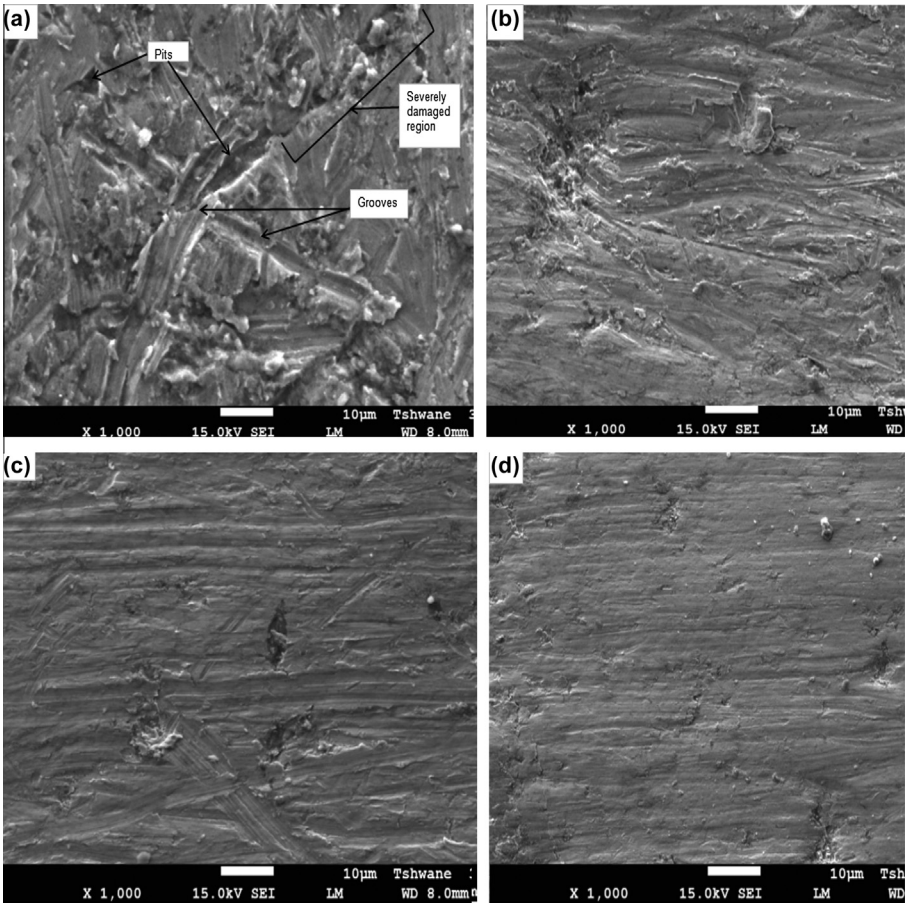

Fig. 7. SEM of the worn surface morphology of: (a) Substrate (as-received Ti–6Al–4V alloy). (b) Sample 1: 50 wt% Mo + 30 wt% Zr + 20 wt% S_6. (c) Sample 2: 30 wt% Mo + 20 wt% Zr + 50 wt% S_6. (d) Sample 3: 20 wt% Mo + 50 wt% Zr + 30 wt% S_6.

Table 3
Calculated standard energy of formation, ΔG_f, of titanium aluminides.

Equation of reaction	Product	ΔG_f (kJ/mol)
3Ti + Al	Ti_3Al	−17.98
Ti + Al	TiAl	9.28
Ti + 2Al	$TiAl_2$	−25.64
2Ti + 5Al	Ti_2Al_5	56.9
Ti + 5Al	$TiAl_3$	−33.7

ages under the three body abrasive loading by a combined effect of majorly adhesive and abrasive mechanism. The native alloy was easily plastically deformed under the combined effects of abrasion by the sand and fatigue due to the repeated action of the wheel. The grooves and the wedge-like shape observed on the wear morphology of the as-received are due to the combine action of abrasion by the sands and fatigue due to cyclic loading by the rubber wheel. The abrasive particle constrained between the wheel and the sample slide on the sample surface to create grooves while material is being pushed to the sides and frontage of the groove. The materials pushed to the side of the groove formed ridges, while the material which was pushed to the frontage of the groove formed wedges. The ridges and wedges became more and larger after the repeated action of the sand and the wheel.

The SEM of the worn surfaces of the coated samples is presented in Fig. 7(b)–(d). The wear behavior of the coatings revealed an improvement in wear resistance in comparison with the uncoated sample, because all the laser coatings exhibited a higher wear resistance. The maximum wear resistance was twenty-four times better than the native alloy, and this was observed in sample 3 which has a powder mixture of 20 wt% Mo + 50 wt% Zr + 30 wt% S_6. This improvement in abrasive wear resistance is obviously due to the homogeneous distribution of the hard molybdenum and tungsten (from stellite 6) in the matrix of the titanium alloy and the good metallurgical bonding of these reinforcement powders with the substrate. However, the sample which has the highest hardness did not yield the best wear resistance. This could be due to the extrinsic properties of wear. Abrasive wear is a complex phenomenon and the materials which have high values for hardness will not necessarily have high resistance to abrasive wear [41].

Similar wear mechanism could be observed from the nature of the wear scar of the coatings, although with varying degrees of deformation which were generally less than that of the AR. This is obviously due to the composition and phases present in alloyed zones, as well as variation in the alloying powder composition. Plastic deformation and micro-fracture of the intermetallic phases is observed in these micrographs (Fig. 7(b)–(d)). The ridge structure of the plastic deformation observed in these micrographs is shallow and non-uniform, and fine scratches predominate. Also evident in the wear morphologies of the coatings are random paths of smearing which were likely caused by the movement of wear debris and abrasive sand during the wear test. As compared to the as-received, the worn surface of the coated layer appeared to be smoother, and no material transfer was observed. This is typical of abrasive wear mechanism. The best wear resistance was obtained from sample 3 which has the highest percentage of Zr. One major difference in phase evolution between sample 1

Table 4
Mechanical properties of the samples.

Sample	Powder composition	Tensile strength (GPa)	Yield strength (GPa)
AR	–	1.22	0.88
1	50 wt% Mo + 30 wt% Zr + 20 wt% S_6	3.73	2.7
2	30 wt% Mo + 20 wt% Zr + 50 wt% S_6	3.33	2.41
3	20 wt% Mo + 50 wt% Zr + 30 wt% S_6	3.24	2.34

(highest hardness) and sample 3 (highest wear resistance) is that the XRD of sample 3 shows the presence of NiV_5 intermetallic (IM) while that of sample 1 shows the presence of NbW IM. The presence of NiV_5 intermetallic phase (sample 3) could be attributed to the dissociation of the stellite 6, and the reaction between the nickel (in the dissociated powder) and the vanadium in the native alloy.

According to Kulu et al. [42] and Hutchings [43], abrasion rate depends on material hardness, and more precisely, on the material hardness/abrasive hardness ratio (H_m/H_a) – if it is lower than abrasive hardness, micro-cutting of the surface may take place. If material hardness is higher than abrasive hardness ($H_m > H_a$), clear removal of the material usually does not take place and the entire process has the nature of fatigue. Hutchings [43] compared the hardness of the abrasive sand, (Ha) to that of the coatings, (Hm) and defined the ratio (Ha/Hm) for abrasive wear system. According to the author, the value of the ratio (Ha/Hm) is used to categorize abrasion as either hard or soft and the boundary value is 1.2. The hardness of the coatings, (Hm), were found to range between 994.7 and 1145.2 HV while the hardness of the abrasive sand, (Ha), can be taken to be 800 HV [43]. Assuming there are no heterogeneities in the coatings and their response to abrasive wear were treated as pure and homogenous, the ratio the hardness of the abrasive sand (Ha) to that of the coatings (Hm), Ha/Hm, is calculated to be 0.7–0.8. This is less than 1.2 – the value which indicates the boundary condition between soft and hard abrasion [43]. This is in agreement with the SEM results. The abrasives sands (SiO_2) are unable to indent and crack the alloyed layers due to these differences in hardness values. The improvement in wear resistance of the laser coated samples is also due to the presence of the titanium aluminides intermetallic (TAI) phases which were precipitated in the MMC. TAI is well known for its ability to resist abrasive wear than Ti and Ti based alloy [44].

The ratio of the force applied per unit area of the sample (pressure) during abrasion can be calculated from the values of the applied load used in the test (25 N) and the area of the sample (420 mm^2). This was found to be 59.52 kPa. This value is theoretical and less than the actual pressure used during the abrasion. This is because the actual area of the sample in contact with the individual grain of the abrasive sand was less than the 420 mm^2 used in the calculation. Using the expression relating the hardness of a material to its tensile and yield strengths as offered by Cahoon et al. [45] in Eqs. (1) and (2) [46], the tensile and yield strengths of the samples were calculated from the hardness results. The results are presented in Table 4. The strain hardening coefficient, n, was taken to be 0.15.

$$TS = \left(\frac{H}{2.9}\right)\left(\frac{n}{0.217}\right)^n \quad (1)$$

$$YS = \left(\frac{H}{3}\right)(0.1)^n \quad (2)$$

The result shows that the applied pressure (59.52 kPa) is far less than the yield strength of the laser coatings. This indicates that the abrasive wear damage of all the laser coatings has been mitigated, and that there is a strong correlation between wear resistance, tensile strength and yield strength of the material. This is in agreement with Oladijo et al. [47].

4. Conclusions

Ti–6Al–4V alloy was successfully laser alloyed with different premixed ratio of Mo + Zr + S_6 The layers obtained consist of fine dendrites of hard titanium aluminides in the matrix of the titanium alloy with α-Ti solid solution present in the interdendritic region. No cracks were observed in the alloyed zone and pores were minimal. The β phase was retained due to the presence of molybdenum (a β-phase stabilizer) in the powder mix. As a result of the fast cooling rate which usually characterizes laser alloying process, some of the β phase were transformed into martensitic α′ which gives higher strength. The reinforcement powders and the precipitated hard titanium aluminide intermetallic and complex phases, led to considerable increase in hardness of the coatings when compared with the as-received. The hardness was increased from 333 $HV_{0.1}$ to about 1145.2 $HV_{0.1}$. Abrasive wear damage was twenty-four times mitigated as the hard reinforcement powder particles and the precipitated intermetallic dendrites constituted a favorable combination in resisting wear damage.

Acknowledgements

This material is based upon work supported financially by the National Research Foundation. The authors also acknowledge the support from the African Laser Centre and the Tshwane University of Technology, Pretoria, South Africa which helped to accomplish this work.

References

[1] Fogagnolo JB, Rodrigues AV, Lima MSF, Amigo V, Caram R. A novel proposal to manipulate the properties of titanium parts by laser surface alloying. J Script Mater 2013;68:471–4.
[2] Wua GQ, Shi CL, Sha W, Sha AX, Jiang HR. Effect of microstructure on the fatigue properties of Ti–6Al–4V titanium alloys. J Mater Des 2013;46:668–74.
[3] Qazi J, Rahim J, Fores FS, Senkov O, Genc A. Phase transformations in Ti6Al4V- *x* H alloys. Metal Mater Trans A 2001;32:2453–63.
[4] Sulekha G, Siddharth G, Ramakrishna A. Titanium: a miracle metal in dentistry. Trends Biomater Artif Org 2013;27:42–6.
[5] Tiana YS, Chena CZ, Chena LB, Chen LX. Study on the microstructure and wear resistance of the composite coatings fabricated on Ti–6Al–4V under different processing conditions. Appl Surf Sci 2006;253:1494–9.
[6] Jianing LI, Chen C, Zhang C. Phase constituents and microstructure of Ti3Al=Fe3Al þTiN=TiB2 composite coating on titanium alloy. Surf Rev Lett 2011;18:103–8.
[7] Guo C, Zhou JS, Zhao JR, Chen JM. Improvement of the tribological properties of pure Ti by laser cladding intermetallic compound composite coating. Proc Inst Mech Eng Eng Tribul 2011;225:864–74.
[8] Momin O, Shana SZ, Yilbas BS. Laser heating of titanium and steel: phase change at the surface. Int J Therm Sci 2012;54:230–41.
[9] Ochonogor OF, Meacock C, Abdulwahab M, Pityana S, Popoola API. Effects of Ti and TiC ceramic powder on laser-cladded Ti–6Al–4V in situ intermetallic composite. J Appl Surf Sci 2012;263:591–6.
[10] Guo C, Zhou J, Zhao J, Wang L, Yu Y, Chen J, et al. Improvement of the oxidation and wear resistance of pure Ti by laser-cladding Ti_3Al coating at elevated temperature. J Tribol Lett 2011;42:151–9.
[11] Liu X, Chu PK, Ding C. Surface modification of titanium, titanium alloys, and related materials for biomedical applications. Mater Sci Eng R 2004;47:49–121.
[12] Lin YC, Lin YC, Chen YC. Evolution of the microstructure and tribological performance of Ti–6Al–4V cladding with TiN powder. J Mater Des 2012;36:584–9.
[13] Chikarakara E, Naher S, Brabazon D. High speed laser surface modification of Ti–6Al–4V. J Surf Coat Technol 2012;206:3223–9.
[14] Adebiyi DI, Popoola API, Pityana SL. Microstructural evolution at the overlap zones of 12Cr martensitic stainless steel laser alloyed with TiC. J Opt Laser Technol 2014;61:15–23.
[15] Wei L, Huijun Y, Chuanzhong C, Diangang W, Fei W. Microstructures of hard coatings deposited on titanium alloys by laser alloying technique. J Surf Rev Lett 2013;20:1–6.

[16] Yakovlev A, Bertrand P, Smurov I. Laser cladding of wear resistant metal matrix composite coatings. Thin Solid Films 2004;453:133–8.
[17] Poulon-Quintina A, Watanabe I, Bertranda C, Watanabe E. Microstructure and mechanical properties of surface treated cast titanium with Nd:YAG laser. Dent Mater 2012;28:945–51.
[18] Zhou R, Sun GF, Chen KK, Tong YQ. Effect of tempering on microstructure and mechanical properties of cast iron rolls laser alloyed with C-B-W-Cr. In: Proceedings of the global conference on polymer and composite materials; 2014.
[19] Sugioka K, Cheng Y. Ultrafast lasers—reliable tools for advanced materials processing. Light Sci Appl 2014:3–30.
[20] Fallah V, Corbin SF, Khajepour A. Process optimization of Ti–Nb alloy coatings on a Ti–6Al–4V plate using a fiber laser and blended elemental powders. J Mater Proc Technol 2010;210(14):2081–7.
[21] Chun G, Zhou J, Zhao J, Wang L, Youjun Y, Chen J, et al. Improvement of the oxidation and wear resistance of pure Ti by laser-cladding Ti_3Al coating at elevated temperature. Tribol Lett 2011;42(2):151–9.
[22] Popoola API, Ochonogor OF, Abdulwahab M. Corrosion and hardness characteristic of laser surface modified Ti6Al4V/Zr + TiC and Ti6Al4V/Ti + TiC. Int J Electrochem Sci 2013;8:2449–58.
[23] Ochonogora OF, Meacockb C, Abdulwahaba M, Pityanaab S. Popoola API Effects of Ti and TiC ceramic powder on laser-cladded Ti–6Al–4V in situ intermetallic composite. Appl Surf Sci 2012;263:591–6.
[24] Chikarakara E, Naher S, Brabazon D, Chikarakara E, Naher S, Brabazon D. High speed laser surface modification of Ti–6Al–4V. Surf Coat Technol 2012;206:3223–9.
[25] Chun G, Zhoua J, Zhaoa J, Guoc B, Youjun Y, Zhoua H, et al. Microstructure and friction and wear behavior of laser boronizing composite coatings on titanium substrate. Appl Surf Sci 2011;257:4398–405.
[26] Yongqing FU, Wei J, Batchelor AW. Some considerations on mitigation of fretting damage by the application of surface-modification technologies. J Mater Process Technol 2000;99:231–45.
[27] Wesemann IA, Hoffmann T, Mrotzek, Martin U. Investigation of solid solution hardening in molybdenum alloys. Int J Refract Met Hard Mater 2010;28(6):709–15.
[28] Arockiasamy A, German Randall M, Heaney Donald F, Wang PT, Horstemeyer Mark F, King RL, et al. Effect of additives on sintering response of titanium by powder injection moulding. Powder Metall 2011;54(3):420–6.
[29] Adebiyi DI, Fedotova T, Pityana SL, Popoola API. Improved hardness of laser alloyed X12CrNiMo martensitic stainless steel. Int J Phys Sci 2011;6:3336–46.
[30] Sun S, Durandet Y, Brandt M. Parametric investigation of pulsed Nd:YAG laser cladding of stellite 6 on stainless steel. Surf Coat Technol 2005;194:225–31.
[31] Vander GF. Metallography, Principles and Practice. Materials Park, Ohio: ASM International; 1999.
[32] Poondla N, Srivatsan TS, Patnaik A, Petraroli M. A study of the microstructure and hardness of two titanium alloys: commercially pure and Ti–6Al–4V. J Alloys Comp 2009;486:162–7.
[33] Duarte A, Viana F, Santos HM. As-cast titanium aluminides microstructure modification. Mater Res 1999;2(3):191–5.
[34] Farnia A, Malek GF, Rao JC, Ocelík V, De Hosson JTM. Effect of Ta on the microstructure and hardness of Stellite 6 coating deposited by low power pulse laser treatments. Surf Coat Technol 2012;213:278–84.
[35] Gogia AK. High-temperature titanium alloys. Defence Sci J 2005;55:143–73.
[36] Chien CC. Phase equilibria at Ti–Al interface under low oxygen pressure. J Mater Sci 2014;1:1–11.
[37] Illarionov AG, Popov AA, Grib SV, Elkina OA. Special features of formation of omega-phase in titanium alloys due to hardening. Met Sci Heat Treat 2010;52:9–10.
[38] He T, Xiong Y, Guo Z, Zhang L, Ren F, Volinsky AA. Microstructure and hardness of laser shocked ultra-fine-grained aluminium. J Mater Sci Technol 2011;27:793–6.
[39] Brytan Z, Bonek M, Dobrzański LA. Microstructure and properties of laser surface alloyed PM austenitic stainless steel. J Achiev Mater Manuf Eng 2010;40(1):70–8.
[40] Man HC, Zhang S, Cheng FT. Improving the wear resistance of AA 6061 by laser surface alloying with NiTi. Mater Lett 2007;61:4058–61.
[41] Harrison A, Draughn RA. Abrasive wear, tensile strength, and hardness of dental composite resins. J Prosth Dent 1976;36:395–8.
[42] Kulu P, Tarbe R, Vallikivi A. Abrasive wear of powder materials and coatings. Mater Sci 2005;11:230–4.
[43] Hutchings IM. Tribology: Friction and Wear of Engineering Materials. Edward Arnold; 2002.
[44] Hawk JA, Alman DE. Abrasive wear of intermetallic-based alloys and composites. Mater Sci Eng 1997;239:899–906.
[45] Cahoon JR, Broughton WH, Kutzak AR. The determination of yield strength from hardness measurements. Metall Trans A 1971;2(7):1979–83.
[46] Krishna SC, Gangwar NK, Abhay KJ, Bhanu P. On the prediction of strength from hardness for copper alloys. J Mater 2013:6. article ID 352578.
[47] Oladijo OP, Sacks N, Cornish LA, Venter AM. Effect of substrate on the 3 body abrasion wear of HVOF WC-17 wt.% Co coatings. Int J Refract Met Hard Mater 2012;35:288–94.